Locating and quantifying gas emission sources using remotely obtained concentration data

Bill Hirst* Philip Jonathan† Fernando González del Cueto‡ David Randell§
Oliver Kosut¶

Abstract

We describe a method for detecting, locating and quantifying sources of gas emissions to the atmosphere using remotely obtained gas concentration data; the method is applicable to gases of environmental concern. We demonstrate its performance using methane data collected from aircraft. Atmospheric point concentration measurements are modelled as the sum of a spatially and temporally smooth atmospheric background concentration, augmented by concentrations due to local sources. We model source emission rates with a Gaussian mixture model and use a Markov random field to represent the atmospheric background concentration component of the measurements. A Gaussian plume atmospheric eddy dispersion model represents gas dispersion between sources and measurement locations. Initial point estimates of background concentrations and source emission rates are obtained using mixed ℓ_2-ℓ_1 optimisation over a discretised grid of potential source locations. Subsequent reversible jump Markov chain Monte Carlo inference provides estimated values and uncertainties for the number, emission rates and locations of sources unconstrained by a grid. Source area, atmospheric background concentrations and other model parameters are also estimated. We investigate the performance of the approach first using a synthetic problem, then apply the method to real airborne data from a 1600km^2 area containing two landfills, then a 225km^2 area containing a gas flare stack.

Key Words: remote sensing, inversion, mixture model, MCMC, reversible jump, compressed sensing, methane, gas flux, greenhouse gases, atmospheric gas dispersion

1. Introduction

There is growing interest in developing methods for detecting and locating sources of gas emissions into the atmosphere. Greenhouse gases are of intense interest (e.g. Chen and Prinn [2006], Shakhova et al. [2010]). Other applications include monitoring toxic gas emissions, locating explosives from their volatile emissions (e.g. Bhattacharjee [2008]]) and mapping naturally occurring gas seeps for oil and gas exploration.The extensive literature on inversion (and the related field, compressive sensing, e.g. Donoho [2006]) includes contributions from the statistics, applied mathematics, electrical engineering and physics communities. Sambridge and Mosegaard [2002] reviews the development and application of Monte Carlo methods for inverse problems in the Earth sciences in general and geophysics in particular. Andersen et al. [2003] presents a method for large scale reservoir modelling using Bayesian inversion of geo–electric resistivity data using reversible jump Markov chain Monte Carlo. Rao [2007] reviews source estimation methods for atmospheric releases of toxic agents, including forward modelling (possibly using Bayesian inference) and backward transport modelling, emphasising the need to assess uncertainties in characterisation of sources using atmospheric transport and dispersion models. Recent articles

*Shell Global Solutions International B.V., The Netherlands.
†Shell Technology Centre Thornton, UK.
‡Shell International Exploration and Production, USA.
§Shell Technology Centre Thornton, UK.
¶Laboratory for Information and Decision Systems, Massachusetts Institute of Technology, USA.

relevant to the current work include Senocak et al. [2008], Keats et al. [2007], Long et al. [2010], Rudd et al. [2012] and Gyarmati-Szabo et al. [2011].

In this paper we concentrate on the task of detecting, locating and quantifying the emission rates of sources of a single gas species of interest, methane, using data acquired during development and testing of an airborne system for mapping natural gas seeps in hydrocarbon exploration over areas typically up to 5000 km^2 per flight. We apply the method to concentration measurements from test flights around a flare stack within a modern natural gas processing facility, collected at ranges of up to 5km downwind of sources. We make inferences about source emission rates using gas concentration measurements. The novelty of the current work lies in the tailored application of a combination of standard statistical modelling components and inference tools for inversion in remote sensing.

The layout of the paper is as follows. Motivating landfill and flare stack applications are first described in section 2. Section 3 outlines the modelling procedure and illustrates it in application to a synthetic problem. Application of the method to the landfill and flare stack measurements is described in section 4. Section 5 provides a discussion of findings and suggestions for future development.

A fuller article (Hirst et al.) describing the methodology, its evaluation and field deployment is in preparation.

2. Data

We used an aircraft–mounted sensitive, high precision methane gas sensor to measure a continuous stream of air from the leading edge of a wing – well away from any fuel/lubricant or engine exhaust fumes. The sensor continuously measures gas concentration and passes data to the aircraft's data logging system with other variables of interest. The sensor delivers better than 1 ppb (part per billion by volume) precision concentration data with a response time of approximately 1 second. Flight data are subsequently merged with specialist meteorological data, including additional wind, atmospheric boundary layer depth and auxiliary data: such as the air sample transit time from sample inlet to sensor measurement chamber. The data sets presented here are atypical of normal hydrocarbon seep surveys, in that we know the locations of sources in the survey areas. Consequently, these data sets provide a valuable test of our measurement and analysis procedures.

Atmospheric methane is responsible for one third of the global warming effect of CO_2 despite methane concentrations being approximately 220 times smaller than those of carbon dioxide. There are strong incentives to reduce methane emissions to the atmosphere. The global average atmospheric methane concentration is approximately $1,820$ppb, increasing at approximately 8ppb per annum [Dlugokencky et al., 2009]. Local atmospheric background methane concentration can vary by approximately 20 ppb during daytime due to changes in Atmospheric Boundary Layer (ABL) depth. This layer of the atmosphere effectively contains all ground level emissions for that day. Its growth is driven by solar heating of the ground. It is important to account for the associated changes in local background concentration, so as to more precisely determine that portion of measured concentration attributable to the local sources of interest: since source related concentrations can be comparable to the albeit much longer term changes in background. The top of the ABL constitutes a "ceiling" on vertical transport of gases from the ground, and reduces rate of dilution with downwind distance from the source. This effect is included in the gas dispersion model used to relate measured concentration to source strength using multiple ABL reflection terms.The aircraft must be within the ABL if it is to detect concentrations from ground level sources.

The flare stack flight comprises 8 separate multi–looped circuits of the flare at altitudes

from 150m to 350m AGL; ABL depth is greater than 1500m. Each circuit intersects the plume three times at different angles and ranges so as to probe the 3-D structure of the dispersion plume. Additionally edge detection of the plume serves to establish the in–flight air sample transit time from inlet to sensor ensuring that concentration measurements are assigned to their correct physical location and time. The flare stack is 50m high, situated within a recently completed natural gas processing plant at a coastal location, where winds are intrinsically more variable. The flare is probably burning methane and light hydrocarbons. Photographs of the flare stack show it to be a clean yellow flame, which suggests it is burning at high efficiency [Kearns et al., 2000]. Methane content of a few percent is expected in the escaping residual unburnt gas; this is due to thermal decomposition and incomplete combustion of the fuel-rich hydrocarbon feed [Pekalski et al., 2005].

Wind field information was supplied by the UK Meteorological Office (UKMO) based on a 4km grid region embedded within their global circulation model. Initial UKMO model–based average wind speed and direction are 11ms^{-1} at -243^o. Figure 1 shows the flight track around and in the vicinity of the flare stack; Figure 2 shows measured methane concentrations against time. Inspection of the concentration trace along the track in Figure 1 suggests that the UKMO predicted wind direction is inaccurate for this portion of the flight made late–afternoon over the coastline.

3. Model

3.1 Model form

We seek to locate and quantify emission rates of methane sources and quantify methane background given n observed atmospheric concentration measurements $\mathbf{y} = \{y_i\}_{i=1}^n$ along airborne trajectory $\mathbf{x} = \{\mathbf{x}_i\}_{i=1}^n$. $\mathbf{y}$ is modelled as the sum of a slowly varying background $\mathbf{b} = \{b_i\}_{i=1}^n$ along the trajectory and contributions due to a distributed group of m sources at ground level locations $\mathbf{z} = \{\mathbf{z}_j\}_{j=1}^m$ with emission rates $\mathbf{s} = \{s_j\}_{j=1}^m$ and auxiliary characteristics $\mathcal{C} = \{\mathcal{C}_j\}_{j=1}^m$. Measurements along the trajectory are assumed to be made with independent identically-distributed additive Gaussian errors $\boldsymbol{\epsilon} = \{\epsilon_i\}_{i=1}^n$, with $\epsilon_i \sim N(0, \sigma_\epsilon^2)$. Steady-state gas transport between a source of unit emission rate at location $\mathbf{z}_j$ and measurement location $\mathbf{x}_i$ in wind field $\mathcal{W}$ is given by coupling function $a_{ij} = a(\mathbf{x}_i, \mathbf{z}_j, \mathcal{C}_j; \mathcal{W})$. With $A = \{a_{ij}\}_{i=1,j=1}^{n,m}$, we adopt the model:

$$\mathbf{y} = \mathbf{A}\mathbf{s} + \mathbf{b} + \boldsymbol{\epsilon} \tag{1}$$

Model mis-specification can be diagnosed by analysis of residuals.

The wind field $\mathcal{W}$ is described by wind vector $\mathbf{U}$ at measurement location x, and horizontal and vertical plume opening angles γ_H and γ_V respectively. We approximate coupling $a(x, z, w; \mathbf{U}, \gamma_H, \gamma_V)$ between a unit source of half width w at location z and measurement location x in wind field $\mathcal{W}$ by a Gaussian plume model. The measurement location relative to the plume is expressed in terms of downwind distance δ_R, and horizontal and vertical offsets δ_H and δ_V of measurement location with respect to wind vector. $\sigma_H = \delta_R \tan(\gamma_H) + w$ and $\sigma_V = \delta_R \tan(\gamma_V)$ play the role of plume "standard deviations" in horizontal and vertical directions respectively.

$$a(x, z, w; \mathbf{U}, \gamma_H, \gamma_V) = \frac{1}{2\pi|\mathbf{U}|\sigma_H\sigma_V} \exp\left\{-\frac{\delta_H^2}{2\sigma_H^2}\right\} \times \left\{ \exp\left\{-\frac{(\delta_V - H)^2}{2\sigma_V^2}\right\} + \exp\left\{-\frac{(\delta_V + H)^2}{2\sigma_V^2}\right\} + \exp\left\{-\frac{(2D - \delta_V - H)^2}{2\sigma_V^2}\right\} + \exp\left\{-\frac{(2D - \delta_V + H)^2}{2\sigma_V^2}\right\} \right\} \tag{2}$$

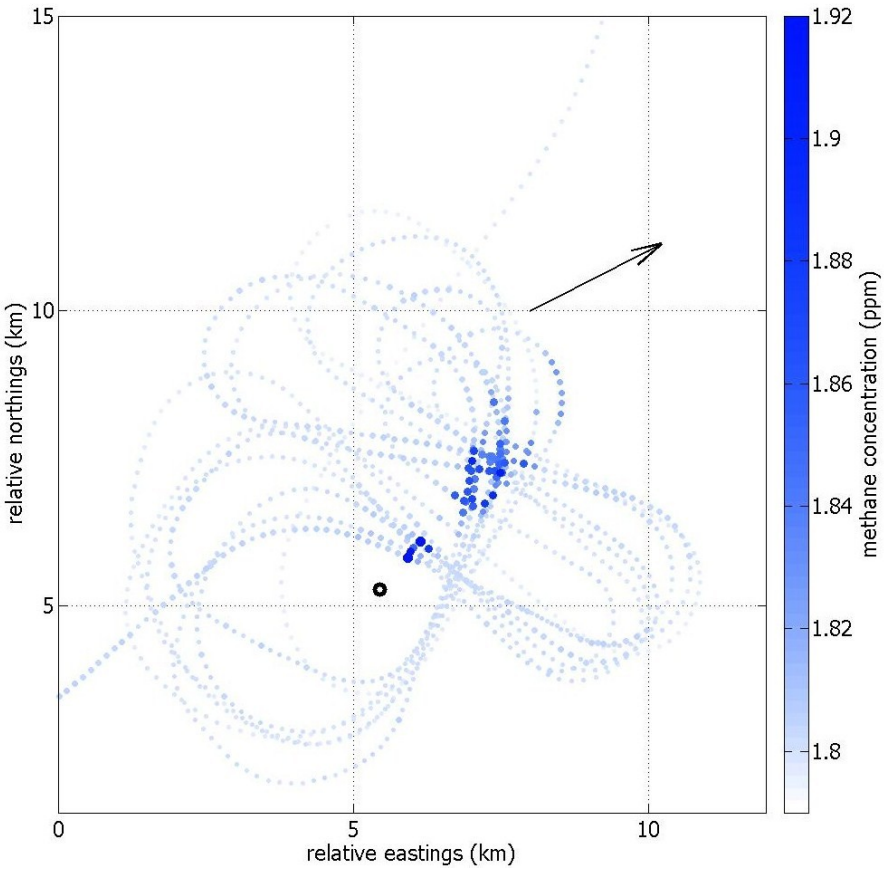

Figure 1: Flight track around and in vicinity of the flare stack. Blue marker size and colour saturation indicate strength and location of measured methane concentrations. Arrow shows average direction of predicted air movement during flight. Black annulus indicates location of flare. The visible discrepancy in alignment of significant concentrations and flare stack with respect to arrow indicates error in predicted direction of air movement. The aircraft enters from the SW corner and leaves to the NE corner.

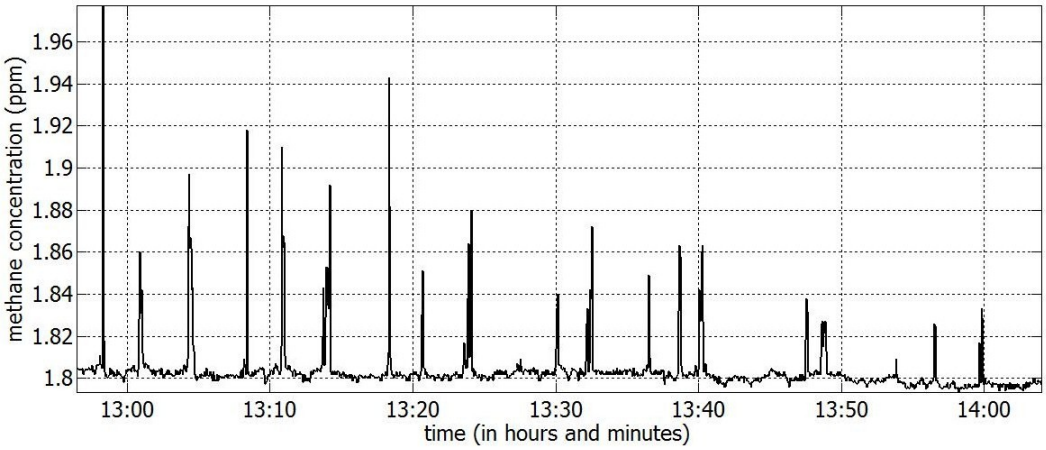

Figure 2: Methane concentrations along flare stack flight path as a function of time.

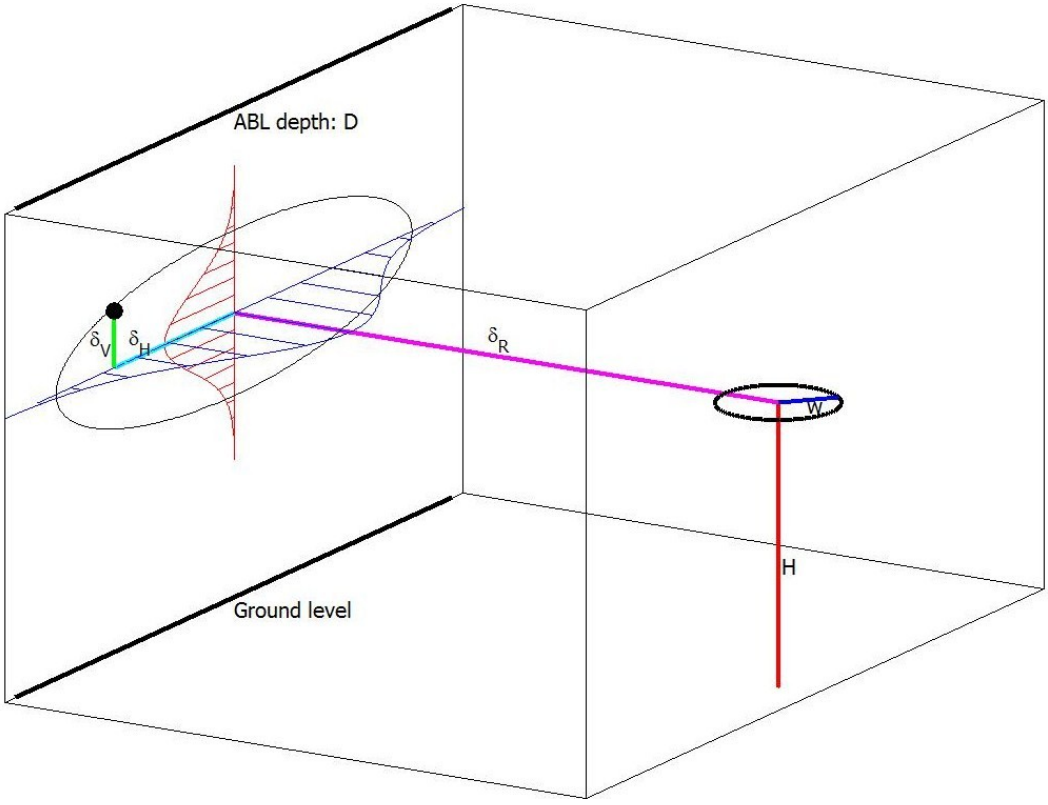

Figure 3: Illustration of plume model parameters. Red line: source height H. Magenta line: downwind distance δ_R of measurement location relative to the source. Cyan line: horizontal offset δ_H. Green line: vertical offset δ_V. Blue line: source half width w. Thick black horizontal lines perpendicular to wind direction represent ground level and top of ABL at height D. The current plume model allows for reflections from ground and ABL ceiling. In this figure δ_R is too short for reflections to be effective. The hatched blue area represents the marginal variation with δ_H of the value of a for $\delta_V = 0$ and fixed δ_R. The hatched red area represents the marginal variation with δ_V of the value of a for fixed δ_H and δ_R. The locus of the black dot (corresponding to a contour of constant a for fixed δ_R) is drawn as a black closed curve.

where D is the height of the atmospheric boundary layer above ground level (referred to as the atmospheric boundary layer depth). The sum of four exponential terms represents plume reflections in the ground and at the interface between atmospheric boundary layer and free atmosphere above it at altitude D. Values of $\mathbf{U}$, D, γ_H and γ_V are obtained directly from wind field data supplied by UKMO. The plume model parameters are illustrated in Figure 3. Typical plume characteristics are illustrated and discussed in the literature (e.g. Senocak et al. [2008]).

Well-mixed background gas concentration $\mathbf{b}$ along the trajectory is assumed to be positive and smoothly–varying spatially and temporally, modelled using a Gaussian Markov random field. $\mathbf{b}$ is a random vector with prior probability density function:

$$f(\mathbf{b}) \propto \exp\{-\tfrac{\mu}{2}(\mathbf{b}-\mathbf{b}_0)^T(\mathbf{J_b})(\mathbf{b}-\mathbf{b}_0)\} \tag{3}$$

with pre-specified precision matrix $\mathbf{J_b}$ and tuning parameter μ. Due to the random field's conditional independence structure, $\mathbf{J_b}$ is guaranteed to be sparse, allowing efficient parameter estimation.

3.2 Parameter estimation

Given measured concentrations $\mathbf{y}$ on trajectory $\mathbf{x}$ and wind field data $(\{\mathbf{U}(\mathbf{x}_i)\}_{i=1}^n, \gamma_H, \gamma_V)$, initial maximum a-posterior estimates for source emission rates $\mathbf{s}$ and background $\mathbf{b}$ are obtained by assuming a spatial grid of potential source locations (with suitable grid resolution). At each grid location, the source emission rate $\mathbf{s}$ is given a Laplace prior for $\mathbf{s}$ with pre-specified precision $\mathbf{Q}$ and tuning parameter λ:

$$f(\mathbf{s}) \propto \exp\{-\lambda\|\mathbf{Q}\mathbf{s}\|_1\} \tag{4}$$

Applying Bayes theorem by multiplying the Gaussian likelihood corresponding to model 1 with the prior densities for $\mathbf{s}$ and $\mathbf{b}$, maximum a-posteriori parameters are seen to correspond to:

$$\underset{\mathbf{s},\mathbf{b}}{\operatorname{argmin}} \qquad \tfrac{1}{2\sigma_\epsilon^2}\|A\mathbf{s} + P\mathbf{b} - \mathbf{y}\|^2 + \tfrac{\mu}{2}(\mathbf{b}-\mathbf{b}_0)^T J(\mathbf{b}-\mathbf{b}_0) + \lambda\|Q\mathbf{s}\|_1 \tag{5}$$

where terms in μ and λ can be viewed as regularisations that impose background smoothness and source sparsity respectively. We further choose to restrict the domain of source elements such that $\mathbf{s}_j \in [0, s_{\max}]$, and background $\mathbf{b}_i \in [0, y_i + \tau]$ for tolerance τ.

For full parameter estimation, we assume that each of m sources can be represented as a two-dimensional Gaussian kernel located at z_j with half width w_j (corresponding to the standard deviation of the Gaussian) and source emission rate s_j. Using reversible jump Markov chain Monte Carlo (RJMCMC, Green 1995), we treat m as a random variable, and estimate the joint distribution of m and all other model parameters. We can also make inferences about apparent bias and/or uncertainty in wind field parameters and measurement error. Bias-correction of wind direction proves to be important in some applications. RJMCMC for mixtures of univariate Gaussians was considered by Richardson and Green [1997] and extended to multivariate Gaussian mixture models by Zhang et al. [2004].

Writing the parameter set $\{\mathbf{z}, \mathbf{w}, \mathbf{s}, \mathbf{b}\}$ as $\boldsymbol{\theta}$ for brevity, we proceed by judiciously partitioning $\boldsymbol{\theta}$ (to exploit problem structure and ensure reasonable MCMC performance), so that dependent parameters appear in the same subset $\boldsymbol{\theta}_\kappa$ of parameters indexed by κ (see, e.g. Gammermann and Lopez [2006]), and that different sampling techniques (such as Gibbs sampling, see below) can be exploited for different subsets. The conditional posterior distribution of parameter subset $\boldsymbol{\theta}_\kappa$ becomes:

$$f(\boldsymbol{\theta}_\kappa|\mathbf{y}, \boldsymbol{\theta}_{\overline{\kappa}}) \propto f(\mathbf{y}|\boldsymbol{\theta}_\kappa, \boldsymbol{\theta}_{\overline{\kappa}}) f(\boldsymbol{\theta}_\kappa|\boldsymbol{\theta}_{\overline{\kappa}}) \tag{6}$$

where $\boldsymbol{\theta}_{\overline{\kappa}}$ represents the remaining model parameters. Starting from a good point estimate for $\boldsymbol{\theta}$, we use a combination of Metropolis-Hastings (Metropolis et al. 1953 and Hastings 1970) and Gibbs sampling (e.g. Geman and Geman 1984) to generate a Markov chain of points $\boldsymbol{\theta} = \{\mathbf{z}, \mathbf{w}, \mathbf{s}, \mathbf{b}\}$ which converge (after burn–in) to a (dependent) sample from $f(\mathbf{z}, \mathbf{w}, \mathbf{s}, \mathbf{b}|\mathbf{y})$. In this way, for a fixed number m of sources, we can estimate the joint posterior distribution of the model parameters. RJMCMC allows sampling from distributions for which the number of sources m (and hence the total number of model parameters) is not fixed by imposing a detailed balance condition to facilitate "dimension jumping". The Metropolis-Hastings algorithm can be extended to accommodate "birth" of a new source, "death" of an existing source, coalescence of neighbouring sources and source division. The Markov chain will therefore explore estimates of $\mathbf{z}$, $\mathbf{w}$ and $\mathbf{s}$ of different dimensions together with $\mathbf{b}$. Inference can be extended to include estimation of quantities such as the measurement error standard deviation σ_ϵ, bias of wind vector $\mathbf{U}$ and horizontal and vertical plume opening angles γ_H and γ_V. In the analysis reported in section 4, σ_ϵ (see (1)), and additive wind direction bias (used in (2)) are included as model parameters in the Bayesian inference.

4. Application

The survey area is partitioned into an 50×50 grid of $300\text{m} \times 300\text{m}$ cells for initial point estimation. The RJMCMC starting point is chosen by sampling 5 locations from the initial optimisation solution, weighted by emission rate.

Figure 1 shows a clear discrepancy between plume direction and mean wind direction predicted by UKMO wind field data. The mixture model, incorporating a constant wind direction bias parameter, successfully corrects this. Inspection of Figure 1 suggests a prior wind direction bias of approximately -18^o. The corresponding posterior 95% credible interval is estimated to be $[-18.12, -17.2]^o$. This uncharacteristically large wind bias is attributed to the flight being in the late afternoon (as the ABL subsides) and is situated at the coast where winds are inherently less predictable. Estimated source emission rates are summarised in emission rate maps in Figure 4 . Panel a) shows the initial optimisation solution. Panel b) shows the posterior median estimate. We summarise marginal spatial uncertainty in terms of the 2.5% and 97.5% credible values for source emission rates shown in Panels c) and d) respectively. Source emission rates in Figure 4 are estimated using corrected wind directions, otherwise the initial optimisation solution (Panel (a)) would be severely compromised. The posterior median mixture model result (Panel (b)) is very similar. Panel (c) shows that 2.5% credible values from the mixture model are $\leq 0.004 m^3 s^{-1}$. Marginal 97.5% credible values in Panel (d) suggest some uncertainty in flare stack location in the wind direction due to the difficulty of "depth resolution" in a relatively stable wind field.

Figure 5 (a) compares initial point and MCMC background estimates, the latter with with credible intervals. The correspondence is reasonable. Figure 5 (b) compares unexplained residual concentration with measured concentration from initial point solution (red) and MCMC (black). For a good model fit, we expect residuals to be zero–mean and show no relationship to the measured concentration. The MCMC residuals are relatively well distributed around zero. For the initial point solution, residuals corresponding to low measured concentrations close to true background (1800ppb) are small; for larger simulated concentrations, residuals are larger and positive since the Laplace prior over source emission rate (4) penalises source strength, generally resulting in positive residuals. Source locations are constrained to the centres of grid cells for the optimisation solution, but not for the mixture model estimate. The interested reader should note that the case presented is a typical example from a number of simulated cases considered but omitted for brevity.

5. Discussion

Individual model components and inference tools used in this work are commonplace in the statistical modelling literature. The combination of components and tools, pulling together physical constraints with rigourous analysis, has proved useful for the remote sensing applications considered in this work. Nevertheless, to the best of our knowledge, this is one of the first applications of Bayesian inference using reversible-jump MCMC to simultaneous multiple source and smooth spatio–temporal background estimation. The Gaussian plume model is a particularly simple steady–state approximation to dispersion of a gas release into the atmosphere, widely used in the environmental modelling literature (e.g. Gifford [1976]). In this work, the plume model provides a reasonable basis for estimating known flare stack and landfill locations. However, we find that correcting bias in (predicted) wind directions supplied by UKMO improves inference. There is evidence, in the form of a "ghost" source downwind of the eastern landfill, that a simple bias correction is not adequate for the long transit times of this extreme case, and that a more sophisticated approach (e.g. a slowly varying wind-direction bias) might be beneficial. There is considerable op-

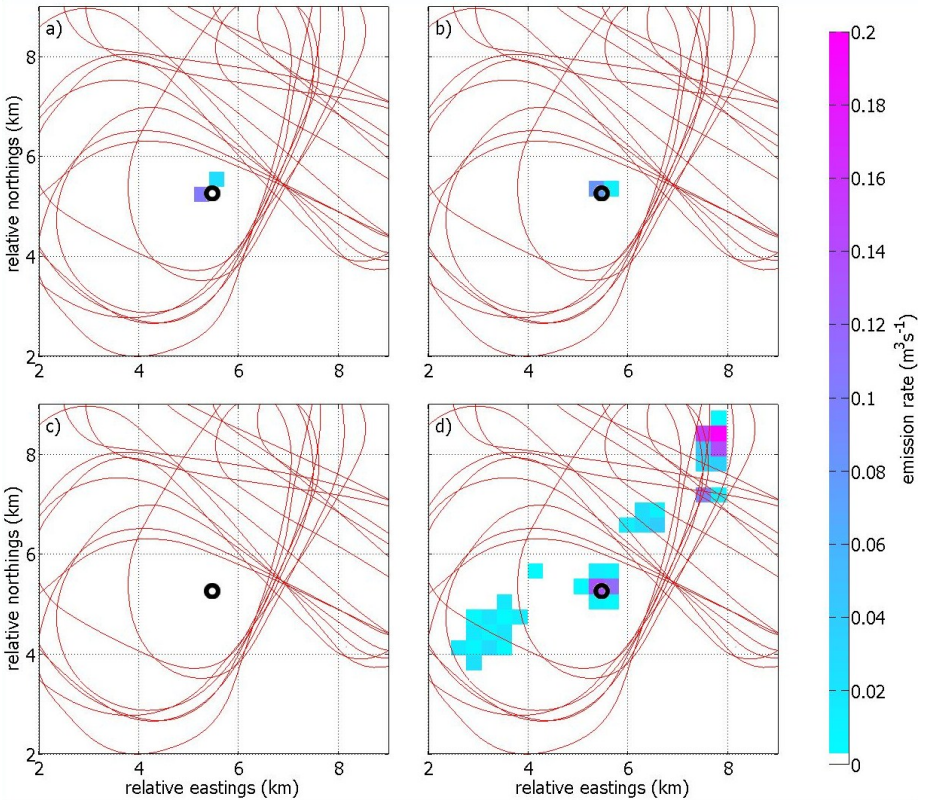

Figure 4: Estimated source emission rate maps for the flare stack application: (a) Estimate from the initial optimisation, (b) Median estimate from the mixture model, (c) Marginal 2.5% credible value from the mixture model, and (d) Marginal 97.5% credible value from the mixture model. All dimensions in km. Emission rates in m^3s^{-1}. Each panel shows a common subregion of the original $15km \times 15km$ domain (referenced with respect to the origin) within which all sources are estimated. For ease of comparison the mixture model results are presented on the same grid cell size as the optimsation solution. The black annulus indicates the location of the flare stack, a point source. The flight path is shown as a red line.

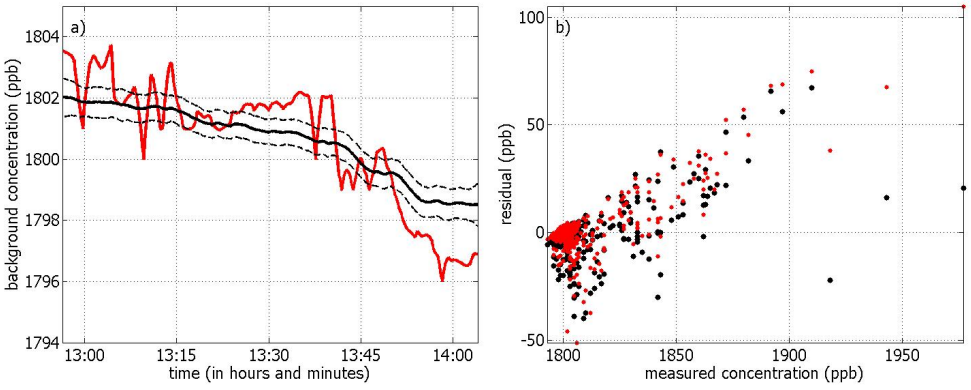

Figure 5: Diagnostics for the flare stack application: (a) Estimated background concentrations along the flight path as a function of time. The initial optimisation is shown in red and the mixture model result is shown in black; median (solid), 2.5% and 97.5% credible values (both dashed) shown. (b) Residuals versus measured methane concentrations from the initial optimisation (red) and median from the mixture model (black).

portunity to achieve this within the Bayesian modelling framework. Incorporating plume model uncertainty in the initial optimisation can be achieved in some sense by considering optimisation over a representative set of forward model matrices A (in Equation (1)), rather than a single choice. Predicated on the availability of wind field data of adequate quality we might also consider more sophisticated plume models, e.g. plumes following wind flow lines, or from computational fluid dynamics. In the MCMC case, we assume a-priori that sources can occur with equal probability at any location. For RJMCMC we sample those grid locations from the optimisation solution with the greatest emission rates as a starting solution. Work continues to explore incorporation of spatial prior distributions for source location, for example using Polya trees to encode some degree of source clustering. There is scope to develop more sophisticated background models incorporating parameters known to influence background methane concentration (such as topography). Our field experience suggests that natural gas seeps can be intermittent, requiring adaptation of our model formulation. Smoothly varying gas release rates could be accommodated relatively simply.

The Gaussian plume model provides an elementary means of modelling gas transport from source to measurement location under ideal steady state wind field assumptions, allowing rapid estimation of forward model matrices A at the expense of accuracy and precision. Given inherent uncertainties in the estimates of wind field parameter values supplied by UKMO, we consider the Gaussian plume adequate for the purposes of the current work. For example in the landfills application, assuming ideal wind field conditions over an interval of approximately 10 minutes for wind speed of approximately 6.5ms^{-1}, suggests that the plume model is appropriate for measurement locations within approximately 4km downwind of a source. More distant measurement locations require ideal conditions over longer periods for the Gaussian plume model to be appropriate. Nevertheless, even over larger distances, the Gaussian plume is likely to provide reasonable approximation to reality provided the wind field remains relatively steady.

As implemented in the current work, optimisation is used to provide an initial point solution for inversion on a spatial grid. Subsequent Bayesian inference gives a more flexible grid-free mixture model framework within which to estimate the joint posterior distribution of all parameters, providing in particular estimates for parameter uncertainty. Early attempts at inversion followed a stepwise approach in which atmospheric background was estimated prior to, and independent of emission sources. The current approach, involving simultaneous estimation of background, sources and wind field characteristics improves performance. We also explored Bayesian inference on the same spatial grid used for the initial optimisation. The very large number of potential source locations makes this computationally intensive.

Our experience of processing multiple survey data sets has made clear the need for rigourous data management and pre-processing procedures. Efficiency of inference can be improved for a given deployment by specifying a flight trajectory (or sequence of flight trajectories) appropriately, given predicted wind conditions and available information concerning likely source locations. Methods of statistical experimental design are central to achieving this for both airborne and ground based line–of–sight gas sensors. It is also strongly desirable to have a means of confirming the quality of inference, particularly of source location and release rate, using a persistent known gas source within the region of interest.

6. Acknowledgement

The authors gratefully acknowledge discussions with colleagues at Shell and at MIT's Laboratory for Information and Decision Systems.

References

KE Andersen, SP Brooks, and MB Hansen. Bayesian inversion of geoelectrical resistivity data. *Journal of the Royal Statisitcal Society B*, 65:619–642, 2003.

Y. Bhattacharjee. Combating terrorism - New efforts to detect explosives require advances on many fronts. *Science*, 320:1416–1417, 2008.

Y.H. Chen and R. G. Prinn. Estimation of atmospheric methane emissions between 1996 and 2001 using a three-dimensional global chemical transport model. *Journal of Geophysical Research-Atmospheres*, 111, 2006.

E.J. Dlugokencky, L. Bruhwiler, J.W.C. White, L.K. Emmons, P. C. Novelli, S. A. Montzka, K. A. Masarie, P. M. Lang, A. M. Crotwell, J. B. Miller, and L. V. Gatti. Observational constraints on recent increases in the atmospheric CH_4 burden. *Geophys. Res. Lett.*, 36, 2009.

D. L. Donoho. Compressed sensing. *IEEE Transactions on Information Theory*, 52:1289–1306, 2006.

D. Gammermann and H. F. Lopez. *MCMC Statistical Simulation for Bayesian Inference*. Chapman and Hall, Boca Raton, 2nd edition, 2006.

S. Geman and D. Geman. Stochastic relaxation, Gibbs distributions and the Bayesian restoration of images. *IEEE Transactions on Pattern Analysis and Machine Intelligence*, 6:721–41, 1984.

F.A. Gifford. Atmospheric dispersion models for environmental pollution. In D.A. Haigen, editor, *Lectures on air pollution and environmental impact analysis*, volume 35-58. American Meteorological Society, Boston, 1976.

P.J. Green. Reversible jump Markov chain Monte Carlo computation and Bayesian model determination. *Biometrika*, 82:711–732, 1995.

J. Gyarmati-Szabo, L. V. Bogachev, and H. Chen. Modelling threshold exceedances of air pollution concentrations via non-homogeneous poisson process with multiple change-points. *Atmospheric Environment*, 45:5493–5503, 2011.

W.K. Hastings. Monte carlo sampling methods using markov chains and their applications. *Biometrika*, 57:97–109, 1970.

B Hirst, P Jonathan, Fernando Gonzalez del Cueto, David Randell, and Oliver Kosut. Locating and quantifying gas emission sources using remotely obtained concentration data. *Atmospheric Environment*. Submitted September 2012.

J Kearns, K Armstrong, L Shirvill, E Garland, C Simon, and J Monopolis. Flaring and venting in the oil and gas exploration and production industry, international association of oil. *Gas Producers Report*, 2.79:288, 2000.

A Keats, E Yee, and F Lien. Bayesian inference for source determination with applications to a complex urban environment. *Atmospheric Environment*, 41:465–479, 2007.

K. J. Long, S E. Haupt, and G. S. Young. Assessing sensitivity of source term estimation. *Atmospheric Environment*, 44:1558–1567, 2010.

N. Metropolis, A. W. Rosenbluth, Teller A. H., and Teller E. equations of state calculations by fast computing machines. *Journal of Chemical Physics*, 21:1087–1092, 1953.

A.A. Pekalski, P. S. D. Smallegange H.P. Schildberg, S. M. Lemkowitz, J. F. Zevenbergen, M. Braithwaite, and H. J. Pasman. Determination of the explosion behaviour of methane and propene in air or oxygen at standard and elevated conditions. *Trans IChemE*, 83: 421–429, 2005.

K. S. Rao. Source estimation methods for atmospheric dispersion. *Atmospheric Environmen*, 41:6964–6973, 2007.

S. Richardson and P. J. Green. On Bayesian analysis of mixtures with an unknown number of components. *Journal of the Royal Statistical Society Series B-methodological*, 59(4): 731–758, 1997.

A. C. Rudd, A. G. Robins, J. J. Lepley, and S. E. Belcher. An inverse method for determining source characteristics for emergency response applications. *Boundary Layer Meteorology*, 144:1–20, 2012.

M. Sambridge and K. Mosegaard. Monte Carlo methods in geophysical inverse problems. *Reviews of Geophysics*, 40:1–29, 2002.

I. Senocak, N W Hengartner, M. B. Short, and W. B. Daniel. Stochastic event reconstruction of atmospheric contaminant dispersion using bayesian inference. *Atmospheric Environment*, 42:7718–7727, 2008.

N. Shakhova, I. Semiletov, A. Salyuk, V. Yusupov, D. Kosmach, and O. Gustafsson. Extensive Methane Venting to the Atmosphere from Sediments of the East Siberian Arctic Shelf. *Science*, 327:1246–1250, 2010.

Z. Zhang, K. L. Chan, Y. Wu, and C. Chen. Learning a multivariate Gaussian mixture model with the reversible jump MCMC algorithm. *Statistics and Computing*, 14:343–355, 2004.